Rapid Nanoimprinting and Excellent Piezoresponse of Polymeric Ferroelectric Nanostructures

Yuanming Liu,[†] Dirk N. Weiss,[‡] and Jiangyu Li[†,*]

[†]Department of Mechanical Engineering, University of Washington, Seattle, Washington 98195-2600 and [‡]Washington Technology Center, Seattle, Washington 98195-2140

ABSTRACT Nanostructured ferroelectric patterns are promising for a wide range of applications, including sensing and actuation, data storage, photonics, spintronics, and energy conversion and storage. In this work, a rapid nanoimprinting technique is developed to pattern ferroelectric poly(vinylidene fluoride-trifluoroethylene) [P(VDF-TrFE)] copolymers in just 3 min, which exhibit excellent ferroelectricity and piezoresponse without any post-imprinting annealing. The effects of imprinting conditions have been thoroughly investigated, and the optimal imprinting parameters for excellent pattern transfer have been identified. The application of the imprinted polymeric patterns as a ferroelectric nonvolatile memory for data storage has also been demonstrated and discussed.

KEYWORDS: nanoimprinting · ferroelectric polymer · piezoresponse force microscopy

Ferroelectric materials are promising for a wide range of applications, including sensing and actuation,[1,2] data storage,[3−6] photonics,[7] spintronics,[8] and energy conversion and storage.[9,10] With the ever-increasing demand for miniaturization of electronic and photonic devices, there have been tremendous efforts in developing nanostructured ferroelectric patterns with smaller feature size, higher density, and improved sensitivity and functionality.[11] Various techniques have been developed to pattern ferroelectric nanostructures, including focused ion beam (FIB) milling,[12−14] E-beam lithography writing,[15] soft lithography,[16] and self-assembling.[17,18] While top-down types of approaches such as FIB milling and E-beam writing are able to create regular arrays of ferroelectric patterns, they are expensive, slow, and difficult to pattern a large area. Defects and damages are often induced during these processes, which tend to degrade the functional properties of ferroelectrics. On the other hand, the bottom-up types of self-assembling approaches usually have poor control over the size and registration of the nanostructures assembled,[19] and thus their practical applications are limited. In recent years, nanoimprinting or nanoimprint lithography (NIL) has emerged as a promising technique for fabricating functional nanostructures,[20−22] and its applications in patterning ferroelectric materials have also been explored.[3,23−28]

Poly(vinylidene fluoride-trifluoroethylene) [P(VDF-TrFE)] copolymer is an excellent class of ferroelectric material with spontaneous polarization close to 10 $\mu C/cm^2$ and piezoelectric coefficient d_{33} around −38 pm/V at room temperature.[1,29−31] While both values are smaller than those of inorganic piezoelectric ceramics, such as lead zirconate titanate (PZT), P(VDF-TrFE) copolymers are advantageous for their excellent solution processability, low annealing temperature, biocompatibility, and they can be easily integrated with both conventional silicon-based microelectronics and emerging organic electronics. As a result, they have been explored for a wide range of device applications, including piezoelectric transducers,[32] organic transistors,[33] electric capacitors,[10] nonvolatile memory cells,[3] and biomedical devices.[34]

Thermal nanoimprinting is a simple process, yet it is able to create nanostructures as small as 5 nm.[20,35] It uses a patterned mold to press against a polymer film heated above its glass transition temperature and thus transfers the pattern from the imprinting mold to the imprinted film. While the process has been applied to pattern ferroelectric polymers, the majority of the nanoimprinting studies focus on the structures imprinted instead of their functional properties. They usually use specially developed nanoimprinting resists instead of functional polymers themselves, and the imprinted nanostructures are often used as masks for further nanofabrication[36] instead

*Address correspondence to jjli@u.washington.edu.

Received for review July 22, 2009 and accepted December 15, 2009.

Published online December 23, 2009. 10.1021/nn901397r

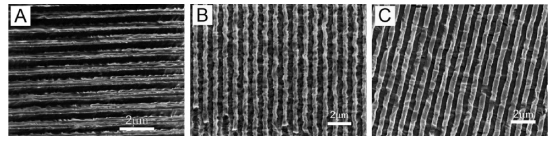

Figure 1. SEM images of imprinted P(VDF-TrFE) patterns using three different molds: (A) hydrophilic silicon mold treated by oxygen plasma, with imprinting temperature of 140 °C; (B) untreated and (C) fluorosilane-coated hydrophobic silicon molds, with imprinting temperature of 150 °C.

of being targeted as the end structure for functional applications. Thus in order to fully realize the potential of nanoimprinted ferroelectric nanostructures, systematic and in-depth studies on nanoimprinting of ferroelectric polymers should be carried out, and the influence of nanoimprinting on ferroelectric properties of the imprinted polymers should be understood.

In this work, we develop a rapid nanoimprinting process to pattern a large area of polycrystalline ferroelectric P(VDF-TrFE) copolymers into regular arrays of ferroelectric patterns and identify the optimal imprinting conditions for efficient and excellent pattern transfer between the imprinting mold and imprinted polymer film. The imprinted pattern has feature size as small as 139 nm, and the imprinting process takes just 3 min, 1 order of magnitude shorter than previous studies on nanomprinting of ferroelectric polymers.[3,26,28] The imprinted patterns show excellent ferroelectric properties and piezoresponse without further annealing after nanoimprinting, a process that is usually required for P(VDF-TrFE) polymers processed from the solution and often takes many hours to complete, much longer than 3 min. In fact, the piezoresponse of nanoimprinted P(VDF-TrFE) patterns is comparable to uniform films annealed in an oven for 12 h and is much larger than films heated in the NIL chamber for 3 min without imprinting. As such, our approach offers a promising route for patterning polymeric ferroelectric nanostructures for a wide range of functional applications.

RESULTS AND DISCUSSION

We first examine the effects of imprinting conditions, such as the mold, temperature, and initial film thickness on the imprinted patterns. P(VDF-TrFE) copolymers are polar in molecular structure and thus tend to be hydrophilic in nature. To examine the effects of mold characteristics on the imprinted patterns, we treat the imprinting mold in three different ways, and the resulted patterns are shown by scanning electron microscopy (SEM) images in Figure 1. The hydrophilic silicon mold, treated by oxygen plasma, is rather difficult to separate from the imprinted film, as we would expect for a hydrophilic mold on a hydrophilic film. The imprinted patterns show many defects, and the surface of the pattern is very rough. On the other hand, the hydrophobic silicon mold, coated with a thin fluorosilane layer [trichloro(1*H*,1*H*,2*H*,2*H*-perfluorooctyl)silane], is

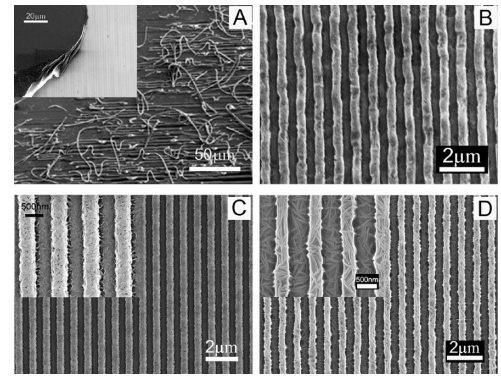

Figure 2. SEM images of P(VDF-TrFE) patterns imprinted at different temperatures: (A) 150 °C, with inset showing the mold after the imprinting; (B) 140 °C; (C) 135 °C, and (D) 130 °C, with inset showing detailed morphology of the polymer.

easily separated from the imprinted film and results in best pattern transfer. The surface of the pattern is also relatively smooth. The untreated silicon mold produces patterns that are similar to those imprinted by the fluorosilane-coated mold with a slightly higher defect density. These observations suggest that fluorosilane-coated silicon molds perform best for nanoimprinting of P(VDF-TrFE) copolymers, and hydrophilic molds cannot produce a satisfactory pattern in P(VDF-TrFE) films.

None of the imprinted patterns in Figure 1 are straight, suggesting that the imprinting temperature is not optimal. The imprinting temperature is very important for ferroelectric polymers because it not only affects the structure of the imprinted films but may also influence their functional properties—a ferroelectric−paraelectric phase transition will occur if the imprinting temperature is higher than the Curie point of P(VDF-TrFE). We examine four different temperatures in our studies, and their effects on the imprinted patterns are shown in Figure 2. It turns out that it is very difficult to separate the mold from the imprinted film at an imprinting temperature of 150 °C, which is evident from Figure 2A, showing that the imprinted pattern is peeled off from the substrate, and part of the imprinted film is attached to the mold, as seen in the inset. With an imprinting temperature of 140 °C, the separation of the mold is much easier, though the imprinted pattern is not straight, similar to those shown in Figure 1B,C. At imprinting temperature of 135 °C, excellent pattern transfer between imprinting mold and imprinted film is observed, with the imprinted patterns being straight and uniform throughout the area. The edge of the pattern appears to be relatively rough, and the higher magnification SEM image shown in the inset suggests that the edge roughness is a result of the polymer morphology itself, instead of from the imprinting process. Such morphology will ultimately limit the resolution of nanoimprinting of ferroelectric polymers. The pattern imprinted at 130 °C is similar to that imprinted

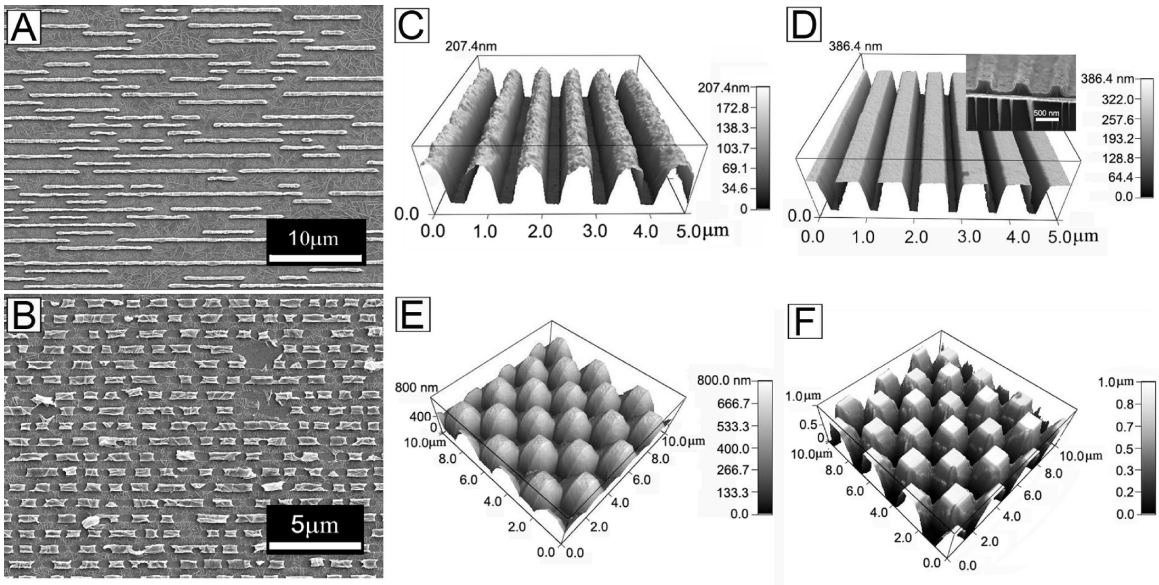

Figure 3. Influence of initial film thickness on the imprinted patterns: (A,B) SEM images of structure imprinted from ultrathin film of 60 nm; (C,D) AFM topography images of one-dimensional line patterns imprinted from (C) 170 nm film and (D) 190 nm film, using a mold with a pattern depth of 200 nm; the inset of (D) showing its SEM cross section image; (E,F) AFM topography images of two-dimensional square pattern imprinted from (E) 300 nm film and (F) 1 μm film, using a mold with a pattern depth of 1 μm.

at 135 °C, and it becomes rather difficult to imprint the polymer at 120 °C. Thus we identify 130−135 °C as the optimal imprinting temperature range for P(VDF-TrFE) copolymers.

An interesting phenomenon we observe in our study is the effect of initial film thickness on the topography of the imprinted patterns, as shown in Figure 3. If we imprint a very thin film of 60 nm, the imprinted pattern is broken into segments, as shown in Figure 3A,B. This could be a result from the loss of stability of thin imprinted patterns at elevated temperature. A similar phenomenon has been reported before in P(VDF-TrFE) films of only a few monolayers thick.[37,38] For thicker films, this does not appear to be a problem, but atomic force microscopy (AFM) images suggest that the topography of the imprinted pattern is greatly influenced by the initial thickness of the imprinted film and pattern depth on the imprinting mold. In order to get a flat top surface of the imprinted pattern, the initial film thickness cannot be much smaller than the pattern depth on the imprinting molds. Otherwise, the imprinted pattern will have a round top surface, with higher center and lower edges. These are evident in Figure 3C, where the initial film thickness is 170 nm and the pattern depth on the mold is 200 nm, and in Figure 3E, where the initial film thickness is 300 nm, and the pattern depth on the mold is 1 μm. For films much thinner than the pattern depth on the mold, the polymer is pushed up by the pressure, yet it cannot touch the bottom surface of the imprinting mold for lack of sufficient materials, resulting in a round top surface for the imprinted patterns because of surface tension. For thicker films, where there are sufficient polymers pushed up to touch the bottom surface of the imprinting mold, a flat top surface is observed in the imprinted pattern. This is clearly seen in Figure 3D, where the initial film thickness is 190 nm and the pattern depth on the mold is 200 nm, and in Figure 3F, where both the initial film thickness and the pattern depth are 1 μm. The inset of Figure 3D shows an SEM cross section image that confirms our analysis: the initial film thickness is 190 nm, and after imprinting, the protruded pattern is around 200 nm high, close to the pattern depth of the mold. A thin residual layer around 70−90 nm thick is observed underneath the imprinted pattern, and such a distribution of protruded pattern and residual layer is consistent with mass conservation analysis for an initially 190 nm thick film.

Some typical P(VDF-TrFE) patterns imprinted with optimal conditions identified in this study are shown in Figure 4. Both two-dimensional square pattern and one-dimensional line patterns are presented, with the finest feature size being 139 nm. Excellent pattern transfers between the molds and the imprinted films have been observed. For these imprinted P(VDF-TrFE) patterns to be useful for functional applications, they must exhibit ferroelectricity and piezoelectricity, and

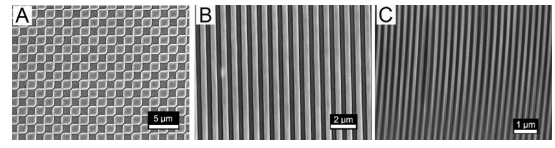

Figure 4. SEM images of typical patterns imprinted at optimal conditions: (A) two-dimensional square pattern; (B) one-dimensional line pattern, with feature size of 417 nm; (C) one-dimensional line pattern, with feature size of 139 nm.

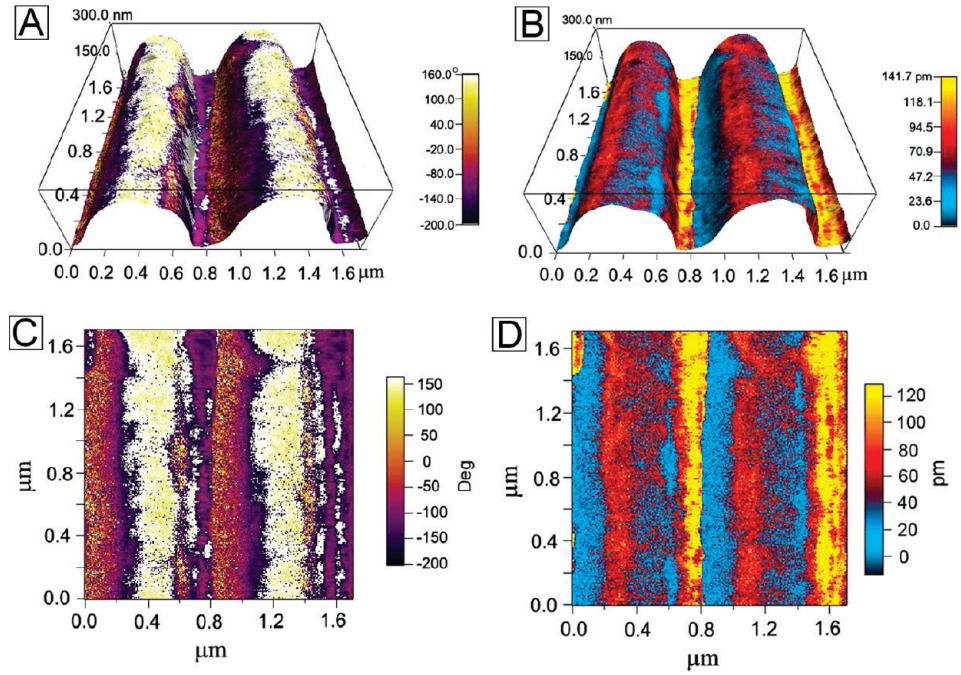

Figure 5. Piezoresponse force microscopy (PFM) of imprinted P(VDF-TrFE) patterns, with an ac driving voltage of 6.6 V: (A) PFM phase image and (B) PFM amplitude image, both imposed on top of the three-dimensional (3D) topography image; the topography is represented by the vertical scale in nanometers, while PFM phase and amplitude are represented by respective color scale bars in degrees or picometers. The corresponding two-dimensional (2D) PFM phase (C) and amplitude (D) images are also shown.

these can be examined by piezoresponse force microscopy (PFM), a scanning probe microscopy (SPM)-based technique developed for unambiguous characterization of ferroelectric materials.[39−41] It applies an ac driving voltage to the specimen through the conductive AFM tip and thus induces a surface vibration if the specimen is piezoelectric. Very often, the ac voltage is driven near the contact resonance of the tip−specimen system to magnify the signal,[42] and such a vibration, or piezoresponse, can be detected through the vibration of AFM cantilever in contact with the specimen surface. The PFM phase indicates the polarity of the piezoelectric coefficient d_{33}, while the PFM amplitude A is proportional to its magnitude, though a quality factor Q ranging from 10 to 100 needs to be multiplied to account for the amplitude enhancement at the tip−specimen resonance, such that $A = d_{33}V_{ac}Q$. For polymer materials such as P(VDF-TrFE), the loss is relatively high, and the quality factor Q is expected to be in the lower end of the range, close to 10. If the specimen is also ferroelectric, then its polarity can be switched by applying a sequence of dc bias imposed on top of the ac driving voltage, and the piezoresponse can be measured as a function of dc bias. This results in a characteristic phase−voltage loop that resembles a polarization hysteresis loop, and an amplitude−voltage loop that resembles a strain butterfly loop. In this paper, we refer such phase−voltage and amplitude−voltage loops as hysteresis and butterfly loops.

For P(VDF-TrFE) copolymers processed from solution, extended period of annealing at around 135 °C is often required to yield the desired ferroelectric β phase. Quite remarkably, even though our film is imprinted at around 135 °C for only 3 min, and there is no post-imprinting annealing process, they still show rather strong piezoelectricity even without poling, as indicated by PFM phase and amplitude images in Figure 5. We believe this is due to the pressure applied during the imprinting, which helps the crystallization of polymers.[25,28] In Figure 5, both three-dimensional (3D) and two-dimensional (2D) images are shown to better illustrate the correlation between imprinted topography and piezoresponse, where in 3D images the piezoresponse (represented by color scale bar in degrees or picometers) is imposed on top of the topography (represented by vertical scale bar in nanometers). Notice that the piezoresponse does not change much along the length of the pattern but varies substantially perpendicular to it, and the highest PFM amplitude is observed in the residual layer at the bottom of the imprinted pattern. This is because at the bottom of the pattern the polymer is subjected to the largest pressure, which tends to align the polymer chains, resulting in enhanced piezoelectricity. With a modest ac driving voltage of 6.6 V, the maximum PFM amplitude is observed over 140 pm, a decent value for an unpoled ferroelectric polymer and comparable to piezoresponse of unpoled uniform films annealed in an oven for 12 h (not shown).

To confirm that the protruded patterns do have good ferroelectricity and piezoresponse, we apply a sequence of dc bias imposed by a 2.2 V ac driving voltage on top of the imprinted square and line patterns and measure the corresponding PFM phase and amplitude, as shown in Figure 6. The ac driving voltage is intentionally reduced to be much smaller than the coercive voltage of the film to avoid interference with switching instability. Between each step of dc bias (state "On"), the dc voltage is stepped back to zero (state "Off"), and piezoresponse is measured at both "On" and "Off" states to better reveal the electric interactions between AFM tip and sample surfaces.[43] Comparisons are also made with uniform films without any annealing, uniform film heated in NIL chamber for 3 min but subjected to no pressing from mold, and uniform film annealed in an oven for 12 h. All of the films were spin-coated under identical conditions, with initial thickness around 600−700 nm. Characteristic hysteresis and butterfly loops are observed in Figure 6A,B under "On" state for imprinted square and line patterns as well as for uniform film annealed in an oven for 12 h. For these films and patterns, PFM amplitude saturates at higher dc voltage, a strong indication that the response is mainly ferroelectric in nature. On the other hand, for films without annealing or heated in NIL chamber for just 3 min without imprinting, the PFM amplitude increases linearly with the applied dc voltage and does not saturate, a strong indication that the response is dominated by electrostatic interactions.[44] To minimize the electrostatic interactions, the hysteresis and butterfly loops in the "Off" state are also measured, as shown in Figure 6C,D, which correlate with true ferroelectricity of the specimens much better. In particular, the linear variation of PFM amplitude with respect to dc bias is no longer present in any of these films. Again, it is noted that the PFM amplitude of nanoimprinted films without additional annealing is essentially comparable to a uniform film annealed for 12 h without imprinting and much larger than that of films without annealing or heated in the NIL chamber for 3 min without imprinting. The amplitudes measured in the "Off" state are generally smaller than those measured in the "On" state (with nanoimprinted square as the only exception), again reflecting minimized contributions from electrostatic interactions. Using the PFM amplitudes measured in the "Off" state at zero dc bias and a quality factor of 10, we estimated the piezoelectric coefficient d_{33} in the range of 48−81 pm/V for nanoimprinted films and annealed uniform film. In contrast, uniform films without annealing or heated in the NIL chamber without imprinting have a piezoelectric coefficient d_{33} in the range of 3−19 pm/V. Furthermore, higher coercive field is observed in the "Off" state than in the "On" state, estimated to be around 25 V for 600−700 nm films. This is comparable to bulk coercive field of 50 mV/m. The difference in coercive field between nanoimprinted films and annealed uniform films is rather small.

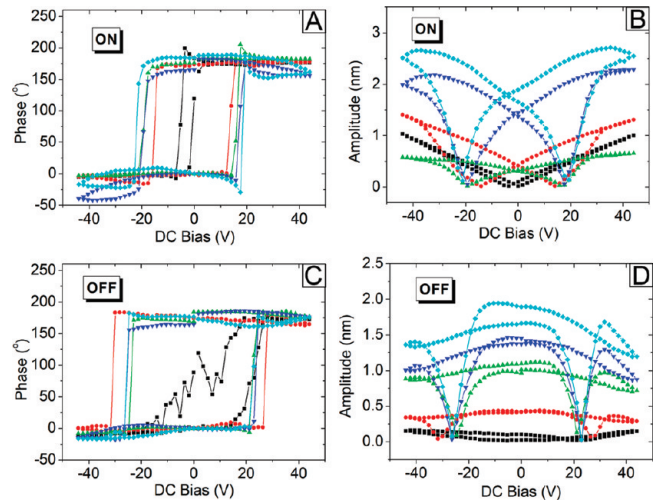

Figure 6. PFM phase−voltage hysteresis loop (A,C) and amplitude−voltage butterfly loop (B,D) of P(VDF-TrFE) films under different processing conditions, in both "On" (AB) and "Off" (CD) states. Different films are denoted by the following legends: ▼ (NIL line); ▲ (NIL square); ◆ (uniform film annealed for 12 h); ● (uniform film heated in NIL chamber for 3 min without imprinting); ■ (uniform film without annealing).

The ferroelectricity of the imprinted patterns enables a number of applications, such as nonvolatile memory cells for the data storage. Here we demonstrate such a concept using the two-dimensional square pattern imprinted, by applying a positive or negative voltage to the conductive AFM tip while scanning over a 20 × 20 μm area in AFM nanolithography mode.[45−47] The tip voltage writes a domain pattern with distribution of positive and negative polarizations, forming a designed pattern of "NIL". Such a pattern can then be read from the PFM phase image, as exhibit in Figure 7A, clearly showing two different phase contrasts, where the phase image is imposed on 3D topography. Before such a poling process, the PFM phase and amplitude images are similar to those shown in Figure 5 and thus are not presented here. It is noted that the writing process does not change the 3D topography, and even more importantly, switching appears to be rather uniform, with no cross-talk observed between adjacent cells. Some of the cells are written into two different phases, suggesting that the writing resolution can be higher than our NIL feature size. It is quite remarkable that, for most area after the writing, the protruded pattern has one uniform PFM amplitude (blue in the amplitude image), and the residual layer has another uniform yet higher PFM amplitude (orange in the amplitude image), as shown in Figure 7B. In other words, within an upward or downward polarization, two different states can be differentiated, corresponding to two different magnitudes of piezoresponse. It is also noted that these written patterns can be rewritten

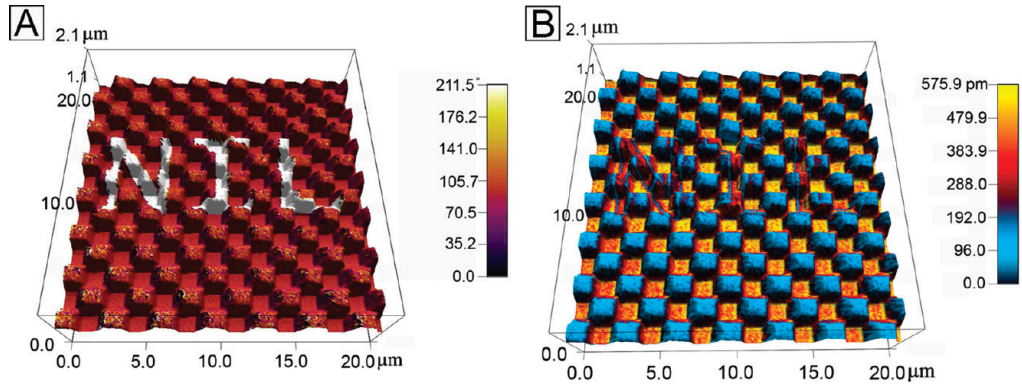

Figure 7. Imprinted ferroelectric film as ferroelectric nonvolatile memory cell, with an "NIL" pattern written by conductive AFM tip and read by PFM: (A) PFM phase image (indicated by color scale bar in degrees), and (B) PFM amplitude image (indicated by color scale bar in picometers), both imposed on 3D topography image (indicated by vertical scale bar in nanometers) of the imprinted film after writing.

by applying a different distribution of positive or negative voltage during scanning.

In summary, we developed a rapid nanoimprinting process to pattern a large area of P(VDF-TrFE) ferroelectric copolymers into regular patterns in just 3 min and identified the optimal imprinting conditions for excellent pattern transfer. The imprinted patterns show excellent ferroelectricity and piezoresponse without post-imprinting annealing, enabling ferroelectric nonvolatile memory cells for data storage. This offers a promising route for patterning polymeric ferroelectric nanostructures for a wide range of functional applications.

METHODS

Materials and Film Preparation: P(VDF-TrFE) copolymer with a molar ratio of 65/35 obtained from Solvay Solexis was dissolved in methyl ethyl ketone (MEK) or dimethylformamide (DMF) and spin-coated onto either a bare silicon substrate or a silicon substrate with 5 nm Ti and 50−100 nm Au evaporated as a bottom electrode for PFM testing. The film thickness, ranging from 60 to 2000 nm, is controlled by adjusting the concentration of P(VDF-TrFE) solution and spin speed and measured by AFM. The film thickness was found to be uniform when the spin speed is over 2000 revolution per minute (rpm), and we choose 3000 rpm for 60 s in all of our experiments. The concentrations of P(VDF-TrFE) are 0.5, 1.0, 2.0, 3.0, 4.0, 5.0, and 10.0% by mass fraction. The spin-coated films are then dried at 80 °C for 30 min. No top electrodes are deposited either before or after the imprinting.

Imprinting Molds and Process: Three types of gratings are used as the imprinting molds: two one-dimensional line gratings obtained from LightSmyth Technologies, Inc. (Eugene, OR), one has a period of 833.3 nm, line width of 416 nm, and pattern depth of 200 nm, and the other has a period of 278 nm, line width of 139 nm, and pattern depth of 110 nm; the third one is a two-dimensional square grating obtained from MikroMasch USA (San Jose, CA) with a period of 3 μm, line width of 1.1 μm, and pattern depth of 1.0 μm. The molds are either untreated and used as received or cleaned by oxygen plasma etching for 3 min to produce a hydrophilic surface or cleaned by oxygen plasma etching for 3 min followed by vapor deposition of a layer of trichloro(1*H*,1*H*,2*H*,2*H*-perfluorooctyl)silane (97%, Sigma-Aldrich Inc., Saint Louis, MO) in a vacuum desiccator to create a hydrophobic surface. The imprinting is conducted on a Nanonex NX-B100 Nanoimprinter using air cushion press technology.[48] Imprinting temperatures are 130, 135, 140, and 150 °C, and the imprinting pressure is chosen to be 300 psi. Heating from room temperature to imprinting temperature takes 6 to 10 s. The imprinting temperature and pressure are held constant for 3 min. The temperature is then reduced to room temperature in about 20 s, after which the pressure is released.

Structure and Property Characterizations: SEM (FEI Sirion) is used to examine the morphology and cross section of the imprinted films, with a 7 nm thick layer of Au/Pd sputtered on the films to avoid surface charging. The surface topography of imprinted film is examined using an Asylum Research MFP-3D AFM and Olympus ac 240TS cantilever in tapping mode. The piezoresponse and ferroelectricity are examined using the high voltage PFM module of MFP-3D AFM and AC 240TM cantilever made of a tetrahedral silicon tip coated with platinum/titanium for conductivity. To image the piezoresponse, ac driving voltage ranging from 1.1 to 8.4 V is applied without a dc bias. To switch the polarization, a sequence of dc bias is applied, forming a triangle wave. The whole cycle takes 100 steps to complete. Between each voltage step, the dc bias is stepped back to zero.

Acknowledgment. The work is supported by National Science Foundation (CMMI-0727922), University of Washington Royalty Research Fund, and the Space and Naval Systems Center Pacific under Award No N66001-06-1-2017 (any opinions, findings, and conclusions or recommendations expressed in this publication are those of the authors and do not necessarily reflect the views of the Space and Naval Systems Center Pacific). The Asylum Research MFP-3D Atomic Force Microscope was acquired through an ARO DURIP grant (W911NF-08-01-0262). Nanoimprint lithography was carried out at Washington Technology Center Microfabrication Laboratory. The scanning electron microscopy was carried out at University of Washington NanoTech User Facility, a member of the National Nanotechnology Infrastructure Network supported by National Science Foundation. Y.L. also acknowledges partial support of a UIF Fellowship from the Center for Nanotechnology, University of Washington.

REFERENCES AND NOTES

1. Zhang, Q. M.; Bharti, V.; Zhao, X. Giant Electrostriction and Relaxor Ferroelectric Behavior in Electron-Irradiated Poly(vinylidene fluoride-trifluoroethylene) Copolymer. *Science* **1998**, *280*, 2101–2104.
2. Li, J. Y.; Rogan, R. C.; Ustundag, E.; Bhattacharya, K. Domain Switching in Polycrystalline Ferroelectric Ceramics. *Nat. Mater.* **2005**, *4*, 776–781.
3. Hu, Z. J.; Tian, M. W.; Nysten, B.; Jonas, A. M. Regular Arrays of Highly Ordered Ferroelectric Polymer Nanostructures for Non-Volatile Low-Voltage Memories. *Nat. Mater.* **2009**, *8*, 62–67.
4. Scott, J. F. Applications of Modern Ferroelectrics. *Science* **2007**, *315*, 954–959.

5. Liao, L.; Fan, H. J.; Yan, B.; Zhang, Z.; Chen, L. L.; Li, B. S.; Xing, G. Z.; Shen, Z. X.; Wu, T.; Sun, X. W.; Wang, J.; Yu, T. Ferroelectric Transistors with Nanowire Channel: Toward Nonvolatile Memory Applications. *ACS Nano* **2009**, *3*, 700–706.
6. Clemens, S.; Rohrig, S.; Rudiger, A.; Schneller, T.; Waser, R. Embedded Ferroelectric Nanostructure Arrays. *Nanotechnology* **2009**, *20*, 075305.
7. Scott, J. F.; Dawber, M.; Jiang, A. Q.; Morrison, F. D. New Developments in Ferroelectric Thin Films. *Ferroelectrics* **2003**, *286*, 945–957.
8. Chu, Y. H.; Martin, L. W.; Holcomb, M. B.; Gajek, M.; Han, S. J.; He, Q.; Balke, N.; Yang, C. H.; Lee, D.; Hu, W.; Zhan, Q.; Yang, P. L.; Fraile-Rodriguez, A.; Scholl, A.; Wang, S. X.; Ramesh, R. Electric-Field Control of Local Ferromagnetism Using a Magnetoelectric Multiferroic. *Nat. Mater.* **2008**, *7*, 478–482.
9. Li, J. Y.; Zhang, L.; Ducharme, S. Electric Energy Density of Dielectric Nanocomposites. *Appl. Phys. Lett.* **2007**, *90*, 132901.
10. Chu, B. J.; Zhou, X.; Ren, K. L.; Neese, B.; Lin, M. R.; Wang, Q.; Bauer, F.; Zhang, Q. M. A Dielectric Polymer with High Electric Energy Density and Fast Discharge Speed. *Science* **2006**, *313*, 334–336.
11. Li, D. B.; Bonnell, D. A. Controlled Patterning of Ferroelectric Domains: Fundamental Concepts and Applications. *Annu. Rev. Mater. Res.* **2008**, *38*, 351–368.
12. Chang, L. W.; McMillen, M.; Morrison, F. D.; Scott, J. F.; Gregg, J. M. Size Effects on Thin Film Ferroelectrics: Experiments on Isolated Single Crystal Sheets. *Appl. Phys. Lett.* **2008**, *93*, 132904.
13. Nagarajan, V.; Stanishevsky, A.; Ramesh, R. Ferroelectric Nanostructures *via* a Modified Focused Ion Beam Technique. *Nanotechnology* **2006**, *17*, 338–343.
14. Hambe, M.; Wicks, S.; Gregg, J. M.; Nagarajan, V. Creation of Damage-Free Ferroelectric Nanostructures *via* Focused Ion Beam Milling. *Nanotechnology* **2008**, *19*, 175302.
15. Ferris, J. H.; Li, D. B.; Kalinin, S. V.; Bonnell, D. A. Nanoscale Domain Patterning of Lead Zirconate Titanate Materials Using Electron Beams. *Appl. Phys. Lett.* **2004**, *84*, 774–776.
16. Seraji, S.; Wu, Y.; Jewell-Larson, N. E.; Forbess, M. J.; Limmer, S. J.; Chou, T. P.; Cao, G. Z. Patterned Microstructure of Sol−Gel Derived Complex Oxides Using Soft Lithography. *Adv. Mater.* **2000**, *12*, 1421–1424.
17. Nonomura, H.; Nagata, M.; Fujisawa, H.; Shimizu, M. A.; Niu, H.; Honda, K. Structural Control of Self-Assembled $PbTiO_3$ Nanoislands Fabricated by Metalorganic Chemical Vapor Deposition. *Appl. Phys. Lett.* **2005**, *86*, 163106.
18. Wu, Z. Q.; Duan, W. H.; Huang, N. D.; Wu, J.; Gu, B. L. Self-Organization Nanodomain Structure in Ferroelectric Ultrathin Films. *Nanotechnology* **2007**, *18*, 325703.
19. Li, J. Y.; Du, Q. G.; Ducharme, S. Regulating Self-Organizing Nanostructures *via* External Mechanism. *J. Appl. Phys.* **2008**, *104*, 094302.
20. Chou, S. Y.; Krauss, P. R.; Renstrom, P. J. Nanoimprint Lithography. *J. Vac. Sci. Technol., B* **1996**, *14*, 4129–4133.
21. Ding, Y. F.; Ro, H. W.; Alvine, K. J.; Okerberg, B. C.; Zhou, J.; Douglas, J. F.; Karim, A.; Soles, C. L. Nanoimprint Lithography and the Role of Viscoelasticity in The Generation of Residual Stress in Model Polystyrene Patterns. *Adv. Funct. Mater.* **2008**, *18*, 1854–1862.
22. Ahn, S. H.; Guo, L. J. Large-Area Roll-to-Roll and Roll-to-Plate Nanoimprint Lithography: A Step toward High-Throughput Application of Continuous Nanoimprinting. *ACS Nano* **2009**, *3*, 2304–2310.
23. Harnagea, C.; Alexe, M.; Schilling, J.; Choi, J.; Wehrspohn, R. B.; Hesse, D.; Gosele, U. Mesoscopic Ferroelectric Cell Arrays Prepared by Imprint Lithography. *Appl. Phys. Lett.* **2003**, *83*, 1827–1829.
24. Hsieh, K. C.; Chen, H. L.; Lin, C. H.; Lee, C. Y. Directly Patterning Ferroelectric Films by Nanoimprint Innography with Low Temperature and Low Pressure. *J. Vac. Sci. Technol., B* **2006**, *24*, 3234–3238.
25. Hu, Z. J.; Baralia, G.; Bayot, V.; Gohy, J. F.; Jonas, A. M. Nanoscale Control of Polymer Crystallization by Nanoimprint Lithography. *Nano Lett.* **2005**, *5*, 1738–1743.
26. Zhang, L.; Ducharme, S.; Li, J. Microimprinting and Ferroelectric Properties of Poly(vinylidene fluoride-trifluoroethylene) Copolymer Films. *Appl. Phys. Lett.* **2007**, *91*, 172906.
27. Chen, H. L.; Hsieh, K. C.; Lin, C. H.; Chen, S. H. Using Direct Nanoimprinting of Ferroelectric Films to Prepare Devices Exhibiting Bi-directionally Tunable Surface Plasmon Resonances. *Nanotechnology* **2008**, *19*, 435304.
28. Kang, S. J.; Park, Y. J.; Hwang, J.; Jeong, H. J.; Lee, J. S.; Kim, K. J.; Kim, H. C.; Huh, J.; Park, C. Localized Pressure-Induced Ferroelectric Pattern Arrays of Semicrystalline Poly(vinylidene fluoride) by Microimprinting. *Adv. Mater.* **2007**, *19*, 581–586.
29. Bune, A. V.; Fridkin, V. M.; Ducharme, S.; Blinov, L. M.; Palto, S. P.; Sorokin, A. V.; Yudin, S. G.; Zlatkin, A. Two-Dimensional Ferroelectric Films. *Nature* **1998**, *391*, 874–877.
30. Omote, K.; Ohigashi, H.; Koga, K. Temperature Dependence of Elastic, Dielectric, and Piezoelectric Properties of "Single Crystalline" Films of Vinylidene Fluoride Trifluoroethylene Copolymer. *J. Appl. Phys.* **1997**, *81*, 2760–2769.
31. Nishio, T.; Miyato, Y.; Kobayashi, K.; Ishida, K.; Matsushige, K.; Yamada, H. The Effect of Local Polarized Domains of Ferroelectric P(VDF/TrFE) Copolymer Thin Film on a Carbon Nanotube Field-Effect Transistor. *Nanotechnology* **2008**, *19*, 035202.
32. Lum, P.; Greenstein, M.; Grossman, C.; Szabo, T. L. High-Frequency Membrane Hydrophone. *IEEE Trans. Ultrason. Ferroelectr. Freq. Control* **1996**, *43*, 536–544.
33. Kim, D. W.; Kim, J. H.; Kim, J. N.; Park, H. J.; Jeon, H. S.; Park, B. E. Characterization of Metal-Ferroelectric-Semiconductor Structure Using Ferroelectric Polymer Polyvinylidene Fluoride-trifluoroethylene (PVDF-TrFE) (51/49). *Integr. Ferroelectr.* **2008**, *98*, 121–127.
34. Li, C. Y.; Wu, P. M.; Lee, S.; Gorton, A.; Schulz, M. J.; Ahn, C. H. Flexible Dome and Bump Shape Piezoelectric Tactile Sensors Using PVDF-TrFE Copolymer. *J. Microelectromech. Syst.* **2008**, *17*, 334–341.
35. Austin, M. D.; Ge, H. X.; Wu, W.; Li, M. T.; Yu, Z. N.; Wasserman, D.; Lyon, S. A.; Chou, S. Y. Fabrication of 5 nm Linewidth and 14 nm Pitch Features by Nanoimprint Lithography. *Appl. Phys. Lett.* **2004**, *84*, 5299–5301.
36. Maury, P.; Peter, M.; Mahalingam, V.; Reinhoudt, D. N.; Huskens, J. Patterned Self-Assembled Monolayers on Silicon Oxide Prepared by Nanoimprint Lithography and Their Applications in Nanofabrication. *Adv. Funct. Mater.* **2005**, *15*, 451–457.
37. Li, J. Y.; Luo, Y.; Bai, M. J.; Ducharme, S. Nanomesa and Nanowell Formation in Langmuir−Blodgett Polyvinylidene Fluoride Trifluoroethylene Copolymer Films. *Appl. Phys. Lett.* **2005**, *87*, 213116.
38. Li, J. Y.; Luo, Y.; Bai, M. J.; Ducharme, S. A Continuum Model on the Nanomesa and Nanowell Formation in Langmuir−Blodgett Ferroelectric Polymeric Films. *J. Mech. Phys. Solids* **2006**, *54*, 2162–2182.
39. Kalinin, S. V.; Bonnell, D. A. Imaging Mechanism of Piezoresponse Force Microscopy of Ferroelectric Surfaces. *Phys. Rev. B* **2002**, *65*, 125408.
40. Kalinin, S. V.; Rar, A.; Jesse, S. A Decade of Piezoresponse Force Microscopy: Progress, Challenges, and Opportunities. *IEEE Trans. Ultrason. Ferroelectr. Freq. Control.* **2006**, *53*, 2226–2252.
41. Gruverman, A.; Kalinin, S. V. Piezoresponse Force Microscopy and Recent Advances in Nanoscale Studies of Ferroelectrics. *J. Mater. Sci.* **2006**, *41*, 107–116.
42. Rodriguez, B. J.; Callahan, C.; Kalinin, S. V.; Proksch, R. Dual-Frequency Resonance-Tracking Atomic Force Microscopy. *Nanotechnology* **2007**, *18*, 475504.
43. Jesse, S.; Baddorf, A. P.; Kalinin, S. V. Switching Spectroscopy Piezoresponse Force Microscopy of Ferroelectric Materials. *Appl. Phys. Lett.* **2006**, *88*, 062908.
44. Hong, S.; Woo, J.; Shin, H.; Jeon, J. U.; Pak, Y. E.; Colla, E. L.;

Setter, N.; Kim, E.; No, K. Principle of Ferroelectric Domain Imaging Using Atomic Force Microscope. *J. Appl. Phys.* **2001**, *89*, 1377–1386.
45. Kalinin, S. V.; Bonnell, D. A.; Alvarez, T.; Lei, X. J.; Hu, Z. H.; Shao, R.; Ferris, J. H. Ferroelectric Lithography of Multicomponent Nanostructures. *Adv. Mater.* **2004**, *16*, 795–799.
46. Li, D. B.; Strachan, D. R.; Ferris, J. H.; Bonnell, D. A. Polarization Reorientation in Ferroelectric Lead Zirconate Titanate Thin Films with Electron Beams. *J. Mater. Res.* **2006**, *21*, 935–940.
47. Rankin, C.; Chou, C. H.; Conklin, D.; Bonnell, D. A. Polarization and Local Reactivity on Organic Ferroelectric Surfaces: Ferroelectric Nanolithography Using Poly(vinylidene fluoride). *ACS Nano* **2007**, *1*, 234–238.
48. Gao, H.; Tan, H.; Zhang, W.; Morton, K.; Chou, S. Y. Air Cushion Press for Excellent Uniformity, High Yield, and Fast Nanoimprint Across a 100 mm Field. *Nano Lett.* **2006**, *6*, 2438–2441.